J Solid State Electrochem
DOI 10.1007/s10008-014-2619-4

ORIGINAL PAPER

Redox transformations in electroactive polymer films derived from complexes of nickel with SalEn-type ligands: computational, EQCM, and spectroelectrochemical study

Vladimir V. Sizov · Maria V. Novozhilova · Elena V. Alekseeva · Mikhail P. Karushev · Aleksander M. Timonov · Svetlana N. Eliseeva · Aleksandr A. Vanin · Valery V. Malev · Oleg V. Levin

Received: 28 March 2014 / Revised: 19 August 2014 / Accepted: 20 August 2014

Abstract Polymer complexes of nickel with SalEn-type ligands (SalEn=*N*,*N*′-bis (salicylidene) ethylenediamine) possess a number of unique properties, such as high redox conductivity, electrochromic behavior and selective catalytic activity in heterogeneous reactions. However, the mechanism of their redox transformation is still not clear. To understand this mechanism, we have performed a combined study of electrochemical and spectral properties of polymers derived from nickel complexes with various SalEn-type ligands containing methoxy substituents in phenyl rings, and methyl substituents in imino bridges. Experimental data were correlated with the results of density functional theory (DFT) calculations for model chains consisting of one to four monomer units. We found that, in acetonitrile-based supporting electrolyte, oxidation of such complexes, regardless of ligand substituents, proceeds via two routes, leading to formation of two oxidized forms: for the first one, a good correlation between experimental and computation results was observed. It has been demonstrated that positive charge in this form is delocalized in the phenyl moieties of ligand. The second oxidized form is stable only in coordinating solvents at high electrode polarizations and is likely to have the charge localized on the central metal atom, stabilized by axial coordination of solvent molecules. The complicated electrochemical response of each of the polymers that we have studied can be explained in the scope of this model without any additional assumptions by taking into account conversion of one oxidized form into another. Understanding the solvent effect on the oxidation route of the complexes will enable controlling their catalytic properties and stability.

Keywords Conductive polymers · Cyclic voltammetry · Quartz crystal microbalance · DFT calculations · Voltabsorptometry

Introduction

Polymers based on complexes of transition metals with SalEn-type ligands (SalEn=*N*,*N*′-bis (salicylidene) ethylenediamine) have a number of unique properties, such as high redox conductivity, electrochromic behavior, and selective catalytic activity in heterogeneous reactions including electrocatalysis, that make them suitable for application in a variety of systems [1–8]. Ni-based complexes are most important due to a high degree of reversibility of their redox reactions. At the same time, the mechanism of their redox transformation is still not clear. One of the important problems is to understand the distribution of the electron density in the polymer and thus to determine the oxidation state of metal in one electron-oxidized complex. In early works devoted to synthesis and characterization of [Ni(SalEn)] polymers, Ni(II)→Ni(III) transformation was assumed as a key redox process [1–3].

Electronic supplementary material The online version of this article (doi:10.1007/s10008-014-2619-4) contains supplementary material, which is available to authorized users.

V. V. Sizov · M. V. Novozhilova · E. V. Alekseeva · S. N. Eliseeva · A. A. Vanin · V. V. Malev · O. V. Levin (✉)
Institute of Chemistry, St. Petersburg State University, Universitetskii pr. 26, Petrodvorets, 198504 Saint Petersburg, Russian Federation
e-mail: levin@chem.spbu.ru

M. P. Karushev · A. M. Timonov
Department of Chemistry, Herzen State Pedagogical University, 6 Kazanskaya (Plekhanova) st, 191186 Saint Petersburg, Russian Federation

V. V. Malev
Institute of Cytology, Russian Academy of Sciences, Tikhoretsky ave. 4, 194064 Saint Petersburg, Russian Federation

Published online: 02 September 2014

Later, several attempts of direct identification of highly oxidized nickel by magnetic resonance methods have failed and thus ligand-based model of polymer electrooxidation was suggested [9–12]. However, this model does not explain all of the features of studied polymers [13]. Indeed, recent studies of analogous oxidized monomeric SalEn-type complexes bearing 3- and 5-substituents which prevent polymerization shows that such oxidized complexes can be described as Ni(II)-phenoxyl radical complexes instead of Ni(III)-phenolate only if they are oxidized in non-coordinating solvents without additions of exogenous ligands [14–17]. It should be emphasized that the electronic structure of oxidized Ni(II) square-planar macrocycles is sensitive to many factors. For instance, Ni(II)-phenoxyl radical to Ni(III)-phenolate transition was found for oxidized monomeric SalEn-type complexes, associated with temperature decrease [18]. Increasing the rings substituents donor strength decreases participation of nickel orbitals in oxidized SalEn-type complex SOMO [19]. It was proved by in situ electron paramagnetic resonance (EPR) spectroscopy that introduction of exogenous ligands such as pyridine, or highly coordinating solvents (e.g., dimethylformamide) shifts the locus of oxidation to Ni center, stabilizing Ni(III) oxidation state and also preventing polymerization of unsubstituted SalEns [18, 20–23] due to axial coordination of solvent molecules.

For the better-studied oxidized Ni(II) porphyrins, a similar behavior was observed, as well as temperature [24] and exogenous ligand-induced valence tautomerism [25]. It was also found that such relatively weak ligands as CH_3CN, which are commonly used for electrochemical studies of polymeric SalEn-type complexes, induce intramolecular charge transfer in oxidized Ni porphyrins stabilizing Ni(III) oxidation state.

Taking the above considerations into account, one cannot exclude the possibility of a high oxidation state becoming stable for metal in polymeric nickel SalEn-type complexes through coordination of solvent in axial positions if these complexes have been oxidized in acetonitrile solutions. In case of polymeric SalEn-type complexes, phenyl moieties in the neighboring polymer chains can also take the role of exogenous ligands [13, 26].

If a moderate coordinating solvent, such as acetonitrile, plays an important role in stabilization of nickel in high oxidation states, ex situ detection of Ni(III) in dry polymer films by any method will fail due to transformation of Ni(III)-phenolate to the Ni(II)-phenoxyl radical after removing axial ligands. However, as it was shown by Storr et al. [17] by combination of in situ EPR and UV-visible spectroscopy of monomeric SalEn-type complexes, Ni(III) could be detected in situ by characteristic ligand-to-metal charge transfer (LMCT) bands near 500 nm in UV-visible spectra. Existence of the band assigned to the phenolate to phenoxyl radical (ligand-to-ligand) charge transfer (LLCT) (at 900–1,100 nm) in the same spectra can also give direct information on the degree of the radical delocalization, which can be estimated by the Robin-Day classification for understanding the mixed valence system [27]. The intensity of the LLCT band in the near-infrared region is high for a fully delocalized system, while in the case of a fully localized system, there is no characteristic LLCT band.

Both characteristic LMCT and LLCT bands are observed in the case of polymeric [Ni(SalEn)] type complexes [9, 10, 12, 28]. The interpretation of these bands, however, traditionally was different from described above, both of them were attributed to polymer fragments, having a charge delocalized over the phenyl rings. Such assumptions could be verified by time-dependent DFT calculations, which, as we know, have not been done before for [Ni(SalEn)] type polymeric complexes.

In the present work, we have chosen a series of different SalEn-type ligands containing methoxy substituents in phenyl rings, which should increase delocalization of the charge due to the high values of the Taft constant. We also have studied complexes containing methyl substituents in imino bridges which have negligible effect on the electron density, but may introduce some steric obstacles for coordination of solvent and phenyl moieties of the neighboring polymer chains onto the central metal atom (Fig. 1). Assuming the model proposed by Vilas-Boas et al. [9], in which polymeric [Ni(SalEn)]-type complexes are described as conjugated “chained” polymers, we have performed density functional theory (DFT) calculations for model chains consisting of one to four monomeric units. Such calculations give information about charge distribution in neutral and oxidized complexes and help to understand the mechanism of their electrooxidation in scope of such model. Apart from the charge distribution, the calculations provide information on geometry changes during electrooxidation and predict the corresponding UV-visible spectra. Results of DFT calculations are compared with experimental data obtained by cyclic voltammetry, UV-visible spectroscopy, in situ derivative voltabsorptometry, and electrochemical quartz crystal microbalance.

Experimental

Experimental methods

Monomer complexes [Ni(Schiff)] (Fig. 1) were synthesized as described earlier [29]. Electrochemical measurements were made in a three-electrode cell consisting of a working electrode, a counter electrode (platinum plate) and a reference electrode (Ag wire in 0.1 M $AgNO_3$ in acetonitrile). However, for consistency, all the potentials are quoted vs. Ag/AgCl (*aq*. KCl sat.) reference electrode. Polymers were synthesized in the form of thin films on a conducting surface by potentiostatic electropolymerization from a solution

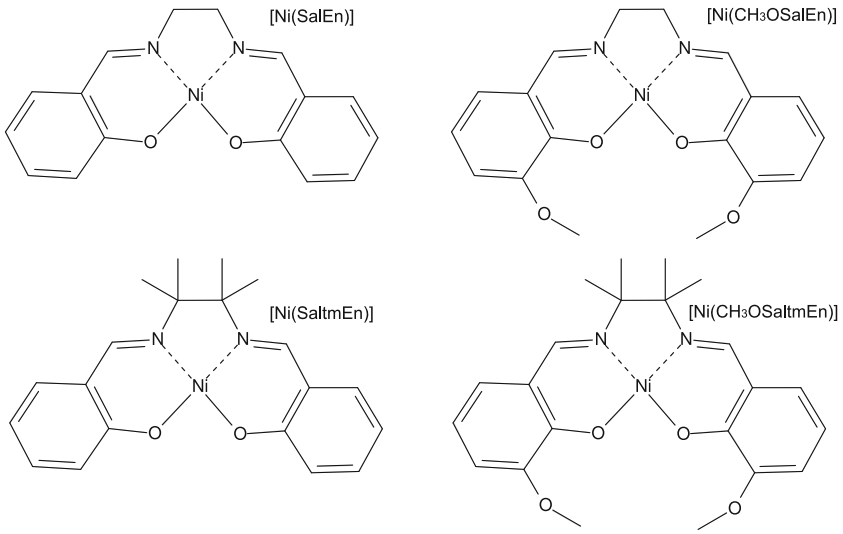

Fig. 1 Molecular structures and abbreviations for the [Ni(Schiff)] complexes used for preparation of polymer films

of 1×10^{-3} M [Ni(Schiff)] and 0.1 M tetraethylammonium tetrafluoroborate N (Et) $_4BF_4$ (Aldrich) in acetonitrile (AN) at the potential of 1 V. We used three types of electrodes to study the properties of the polymers: the glass covered with indium tin oxide (ITO) (surface area of 2 cm^2), 0.07 cm^2 glassy carbon electrode and 5 MHz quartz piezoelectric crystal sprayed with a layer of platinum on an area of 1.37 cm^2. Polymerization charge in each case is equal to 10 mC. Polymerization efficiency was controlled by QCM measurements. Three similar films of each polymer were synthesized on the quartz crystal, dedoped at 0 V, washed carefully by acetonitrile and dried in dry air up to the constant mass under QCM control. Masses of the polymer films determined from QCM data for dry polymers in air medium were within 10 % tolerance with the masses calculated from the polymerization charge assuming a two-electron process. This observation allows us to assume 100 % polymerization efficiency for other experiments. In this case, according to the Faraday law, polymerization charge of 10 mC corresponds to formation of 5.2×10^{-8} mol of polymer, so the surface coverage was 3.8×10^{-8} mol/cm^2 for 1.37 cm^2 QCM crystal and 2.6×10^{-8} mol/cm^2 for 2 cm^2 ITO plate. This corresponds to a film thickness of 100–150 nm, assuming polymer density to be 1 g/cm^3. Studies of electrochemical properties of the polymers were carried out in the background electrolyte, which is the 0.1 M solution of tetraethylammonium tetrafluoroborate $N(Et)_4BF_4$ (Aldrich) in AN. The salt was recrystallized from isopropyl alcohol solution and dried at 120 °C before experiments. Acetonitrile of an HPLC grade was obtained from Kriochrom (Russia) and stored under 3 Å molecular sieves. To perform voltammetric measurements, we used potentiostat/galvanostat Autolab PGSTAT30 (Eco Chemie, Netherlands) and Elins P-30I (Russia). Installation for microgravimetric research contains QCM200 Quartz Crystal Microbalance Analog Controller and QCM25 Crystal Oscillator (Stanford Research Systems, USA) with sensitivity factor of 56.6×10^6 Hz g^{-1} cm^2, which means 1 Hz corresponds to 17.7 ng cm^{-2}. UV-visible absorption spectra were registered by a spectrophotometer Shimadzu UV 1700 (Japan). EQCM measurements were performed in a dry box with water content less then 100 ppm to avoid degradation of the film during the long measurements; spectroscopic studies were carried out on air, but these measurements were fast enough, and no changes of the electrochemical properties of the film were observed during the experiment. Estimation of the effect of changes in film viscoelastic properties on the crystal vibration frequency was done by monitoring the series resonance resistance in EQCM measurements. For all measurements discussed below, the viscoelastic contribution appears to be negligible compared to the effect exerted on the frequency by changes in the polymer weight.

Computational methods

Quantum chemical calculations were performed for isolated $[Ni(Schiff)]_n$ (n=1–4) species to investigate possible changes in the electronic structure of these complexes upon their oxidation. All complexes are assumed to comprise four-coordinated nickel atoms with a near-planar structure of the monomeric units. In oligomeric (n=2, 3, 4) species, the monomeric units are connected by carbon-carbon bonds in *para*-positions of aromatic rings, as assumed in Ref. [9]. It is also assumed that the potentially available axial positions are not occupied by ligands (such as solvent molecules). Since this assumption might have important consequences, the effects of the presence of axial ligands will be reported in more detail elsewhere. In DFT calculations, all molecules were considered to be isolated species, so the potential effects of intermolecular interactions (e.g., interactions of charged complexes with

counterions or interactions of oligomeric fragments with each other) were not taken into account.

A comparison between the results obtained for monomeric and oligomeric species can reveal the effects of polymerization on the electronic structure, including the asymmetry of electron density distribution or the non-equivalence of terminal and central monomeric units in a polymer chain. Furthermore, such study of oligomeric complexes can yield valuable information on the effects of partial oxidation processes, such as $[Ni(Schiff)]_4^0 \rightarrow [Ni(Schiff)]_4^{2+}$. This approach provides a detailed description of electronic structure, which could not be achieved if the computational study was limited to monomeric complexes. A comparison of complexes with the full range of n values (n=1–4) was carried out for $[Ni(SalEn)]_n$ species. The role of methyl substituents in the bridging fragments and CH_3O groups in the aromatic rings was studied for $[Ni(Schiff)]_2$ dimers only.

All quantum chemical calculations were performed using DFT with the B3LYP hybrid functional [30–32]. The LANL2DZ basis set with LANL2 effective core potential [33, 34] was chosen for Ni atoms; the 6–31G(d,p) basis set was accepted for all other atoms. The structures of all monomers and oligomers were fully optimized and verified by calculating vibrational frequencies. Atomic charges were evaluated using Mulliken population analysis. Electronic spectra were obtained from time-dependent DFT (TD-DFT) calculations. All calculations were performed using the Gaussian 09 package [35].

DFT geometry optimizations and TD-DFT calculations were carried out for all [Ni(Schiff)] and $[NiCH_3OSchiff]$ monomers in reduced and oxidized forms, $[Ni(Schiff)]_2$ and $[Ni(CH_3OSchiff)]_2$ dimers in different oxidation states, as well as for $[Ni(SalEn)]_3$ trimers and $[Ni(SalEn)]_4$ tetramers. This variety of species was used to study the effects of polymerization on electronic structure and spectral properties, which cannot be accounted for in scope of the computational study limited to monomers.

Results and discussion

DFT calculations

Geometry and electronic structure

The results of DFT calculations indicate that the electronic density in the complexes considered in this work is strongly delocalized. Table 1 illustrates the involvement of different fragments of the complexes in stepwise oxidation processes. Upon removal of one electron from [Ni(Schiff)] monomeric complexes, the largest contribution is provided by the peripheral rings of the ligand. The substitution of hydrogen atoms in 3-positions by CH_3O groups introduces a strong electron donor to the complex, thereby reducing the contribution of other fragments during the oxidation of the complex. Thus, the introduction of donor groups may significantly facilitate the oxidation of the complex by decreasing the burden on other parts of the complex.

The analysis of atomic charges in $[Ni(Schiff)]_2$ dimeric complexes yields results which are almost identical to those obtained for monomers (Table 1). According to the charge distribution analysis, the $[Ni(Schiff)]_2^0 \rightarrow [Ni(Schiff)]_2^{1+}$ half-oxidation process can be treated with sufficient accuracy as a half of the $[Ni(Schiff)]_2^0 \rightarrow [Ni(Schiff)]_2^{2+}$ process, i.e., the effects of the removal of the first and second electrons from $[Ni(Schiff)]_2$ dimers are almost equal.

The electronic configuration of metal atoms does not undergo noticeable changes upon the oxidation of the complexes. The oxidation state of the nickel atom in both $[Ni(SalEn)]_2^+$ and $[Ni(SalEn)]_2^{2+}$ complexes was identified as Ni(II) according to the near-zero spin density on Ni atoms. This result does not support the perception of the oxidation of [Ni(Schiff)] complexes as a Ni(II)→Ni(III) process. However, a different picture of [Ni(Schiff)] oxidation was observed in DFT calculations when the representation of the complexes was changed from planar four-coordinated Ni to six-coordinated Ni with two solvent molecules in axial positions. Comparison of DFT results for oxidized monomeric complexes $[Ni(SalEn)]^+$ and $[Ni(SalEn)(CH_3CN)_2]^+$ revealed a drastic difference in spin density distribution (Fig. 2). As described above, in four-coordinated $[Ni(SalEn)]^+$ complex, the spin density is delocalized over the Schiff base, leading to the unambiguous description of the nickel atom as Ni(II). For the six-coordinated $[Ni(SalEn)(CH_3CN)_2]^+$ complex, in which the axial positions are occupied by two solvent molecules, the spin density is strongly localized around the metal atom with the total spin density on Ni being equal to 1.1. This result provides sufficient evidence for the interpretation of $[Ni(SalEn)(solvent)_2]$ oxidation as a metal-based Ni(II)→Ni(III) process. A similar effect of the coordination of axial ligands on the nature of the oxidation mechanism has been reported previously [18, 20–22]. In the light of the DFT calculation results obtained for the six-coordinated $[Ni(Schiff)(solvent)_2]$ complex, the nature of the oxidation process requires a more detailed computational study.

The charge distributions for the central and peripheral monomeric units in four-coordinated $[Ni(Schiff)]_3^0$ and $[Ni(Schiff)]_4^0$ oligomers are identical and completely similar to both monomers and dimers. For both trimer and tetramer complexes, upon oxidation of neutral species the peripheral units donate more density than the central ones. Though the process of further oxidation may proceed in somewhat different manner for trimers and tetramers (Table 1), the total contributions of the fragments for complete oxidation (removal of one electron per monomeric unit) of the oligomers are

Table 1 Contributions of fragments (per monomeric unit) to the oxidation processes in $[Ni(Schiff)]_n$ complexes. Electronic density is described using Mulliken charges averaged over the corresponding fragments of the complexes

Oxidation process	Contributions of fragments, *e*					
	Ni	O	N	CH_3O	Rings	Bridge
$[Ni(Schiff)]^q$ monomers						
$[Ni(SalEn)]^0 \rightarrow [Ni(SalEn)]^+$	0.09	0.10	−0.01	–	0.71	0.11
$[Ni(SaltmEn)]^0 \rightarrow [Ni(SaltmEn)]^+$	0.09	0.09	0.01	–	0.68	0.13
$[Ni(CH_3OSalEn)]^0 \rightarrow [Ni(CH_3OSalEn)]^+$	0.06	0.08	0	0.17	0.59	0.10
$[Ni(CH_3OSaltmEn)]^0 \rightarrow [Ni(CH_3OSaltmEn)]^+$	0.06	0.08	0.01	0.16	0.57	0.12
$[Ni(Schiff)]_2^q$ dimers						
$[Ni(SalEn)]_2^0 \rightarrow [Ni(SalEn)]_2^+$	0.04	0.05	0	–	0.35	0.06
$[Ni(CH_3OSalEn)]_2^0 \rightarrow [Ni(CH_3OSalEn)]_2^+$	0.03	0.05	0	0.08	0.29	0.05
$[Ni(SalEn)]_2^+ \rightarrow [Ni(SalEn)]_2^{2+}$	0.04	0.05	0	–	0.35	0.06
$[Ni(CH_3OSalEn)]_2^+ \rightarrow [Ni(CH_3OSalEn)]_2^{2+}$	0.03	0.04	0	0.09	0.29	0.05
$[Ni(Schiff)]_3^q$ trimers						
$[Ni(SalEn)]_3^0 \rightarrow [Ni(SalEn)]_3^+$						
Peripheral	0.03	0.03	0	–	0.21	0.04
Central	0.03	0.04	0	–	0.26	0.05
$[Ni(SalEn)]_3^+ \rightarrow [Ni(SalEn)]_3^{2+}$						
Peripheral	0.03	0.03	0	–	0.26	0.04
Central	0.02	0.03	0	–	0.19	0.04
$[Ni(SalEn)]_3^{2+} \rightarrow [Ni(SalEn)]_3^{3+}$						
Peripheral	0.04	0.04	0	–	0.29	0.04
Central	0.02	0.02	0	–	0.12	0.02
$[Ni(Schiff)]_4^q$ tetramers						
$[Ni(SalEn)]_4^0 \rightarrow [Ni(SalEn)]_4^{2+}$						
Peripheral	0.04	0.05	0	–	0.36	0.07
Central	0.04	0.05	0	–	0.32	0.07
$[Ni(SalEn)]_4^{2+} \rightarrow [Ni(SalEn)]_4^{4+}$						
Peripheral	0.05	0.06	0	–	0.43	0.07
Central	0.03	0.04	0	–	0.27	0.05

quite similar. For the whole $[Ni(Schiff)]_3^0 \rightarrow [Ni(Schiff)]_3^{3+}$ process, the contribution of the central unit is 0.84 *e*, while each of the peripheral units donates 1.08 *e*. For the $[Ni(Schiff)]_4^0 \rightarrow [Ni(Schiff)]_4^{4+}$ process the contributions of central and peripheral units are 0.88 and 1.12 *e*, respectively, which is in good agreement with the results obtained for trimers.

The oxidation of dimeric complexes is also accompanied by structural changes. Upon oxidation of $[Ni(Schiff)]_2^0$ species, the dihedral angle between the monomeric units decreases from 33 to 39° for the reduced form of the complex to ca. 20° for the fully oxidized one (Table 2). In $[Ni(CH_3OSchiff)]_2$ complexes, this effect is somewhat less pronounced. Increasing the size of $[Ni(Schiff)]_n$ oligomers allows for more interesting effects to be observed through DFT calculations, as the monomeric units at the ends and in the middle of the chain are not equal in terms of electronic structure. This non-equivalence of monomeric units is

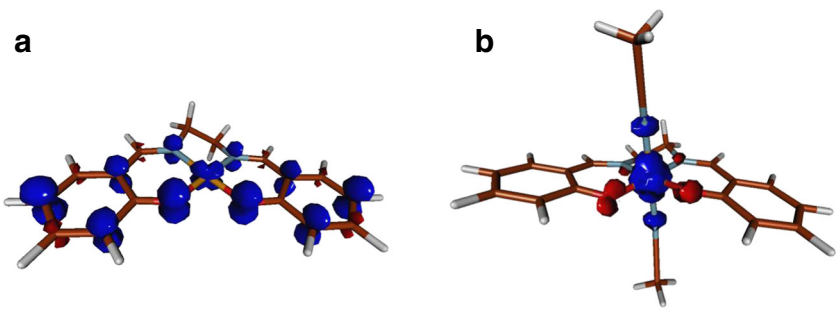

Fig. 2 Spin density distributions for $[Ni(SalEn)]^+$ (**a**) and $[Ni(SalEn)(CH_3CN)_2]^+$ (**b**) complexes obtained from DFT calculations

Table 2 Dihedral angles between [Ni(Schiff)] monomeric units in uncharged and charged $[Ni(Schiff)]_n$ complexes

Charge	Dihedral angles, degrees	
	$[Ni(SalEn)]_2$	$[Ni(CH_3OSalEn)]_2$
0	39	33
1+	22	21
2+	17	21
	$[Ni(SaltmEn)]_2$	$[Ni(CH_3OSaltmEn)]_2$
0	35	35
2+	17	20
	$[Ni(SalEn)]_3$	
0	36	
1+	28	
2+	23	
3+	25	
	$[Ni(SalEn)]_4$	
	Central/peripheral	Central/central
0	36	36
2+	25	29
4+	18	25

especially noteworthy for $[Ni(Schiff)]_4$ tetramers in which two distinct types of dihedrals can be observed: those between two central monomeric units or between a central and a peripheral one. While for $[Ni(SalEn)]_4^0$ all three dihedrals (two of the central/peripheral type and one central/central) are equal within computational accuracy, the oxidation of the complex results in a diversification of dihedral angles with the central/peripheral angles undergoing larger changes than the central/central one. The different behavior of two types of angles is clarified by the analysis of charge transfer in $[Ni(SalEn)]_4$ upon oxidation: since the central fragments donate less electrons, their electronic structure undergoes less significant changes than in the case of peripheral fragments (Table 1). So, the decrease of central/central dihedral is predictably smaller than for central/peripheral ones.

Electronic spectra

A deeper insight into the spectral properties of the complexes studied can be obtained from TD-DFT calculations, which will be used here predominantly for the assignment of bands in UV-visible spectra. The calculated spectrum for the $[Ni(SalEn)]^0$ monomer shows a good agreement with experimental data (Fig. 3).

For the monomer, the low-energy band at 440–450 nm is almost absent, and the high-energy band is noticeably blue-shifted as compared to the dimer and tetramer. The near-absence of the low-energy band at for $[Ni(SalEn)]^0$ can easily be explained if we consider its nature for larger complexes, e.g., for the $[Ni(SalEn)]_2^0$ dimer. This band comprises three

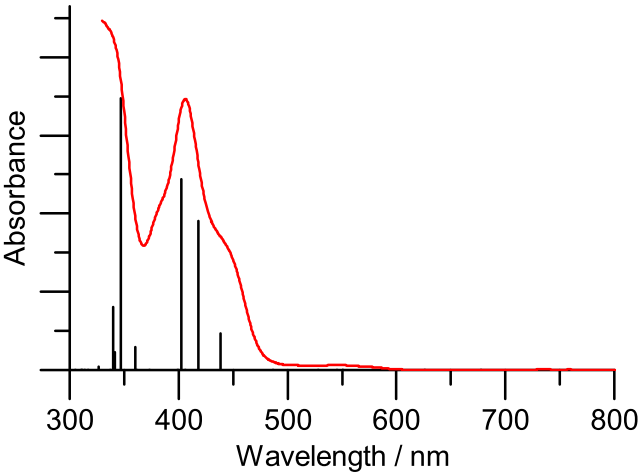

Fig. 3 Electronic spectra obtained for [Ni(SalEn)] monomer from TD-DFT calculations. The curve is experimental spectrum recorded in 0.1 mmol solution of monomer in acetonitrile using standard 1×1 cm photometric cell

transitions, which are interpreted as interligand localization/delocalization transition (451 nm), mixture of MLCT and charge transfer from one monomeric unit to another (438 nm), and a LLCT transition with a small MLCT contribution (431 nm). So, the presence of the low-energy band near 440 nm is largely caused by charge transfer involving more than one monomeric unit, and therefore for monomers this band is likely to have lower intensity or will not be observed at all. The UV band is also represented by a complex mixture of transitions of a different nature (MLCT), but the exchange between monomeric units is less pronounced for these, so the UV band is also observed for the monomer, though its energy is noticeably higher.

As the spectra for monomeric species show significant differences from those for $[Ni(SalEn)]_n^0$ complexes, the effects of oxidation on the spectral properties will be illustrated by TD-DFT calculation results for $[Ni(SalEn)]_4^q$ tetramers (Fig. 4).

The spectra for the oxidized forms feature IR bands: 3,301 nm and 1,758 nm for $[Ni(SalEn)]_4^{2+}$, 2,671 nm, 2,097 nm, and 1,354 nm for $[Ni(SalEn)]_4^{4+}$. All these bands are assigned to the electron density exchange between the aromatic rings of the ligands, i.e., to LLCT transitions. The bands observed for both oxidized forms between 700 and 900 nm are interpreted as LLCT with a weak MLCT contribution. The ligand-ligand exchange predominantly involves the aromatic rings, though interactions between the rings and bridging fragments are also observed. The spectrum of $[Ni(SalEn)]_4^{4+}$ features a group of transitions with a strong metallic character: MLCT (from "outer" metals to "outer" rings) bands with minor contributions at 712 and 655 nm, and a mixed MMCT/MLCT band at 646 nm. The MMCT transition occurs from the "inner" to the "outer" metal atoms. All these bands have substantial LLCT contributions due to

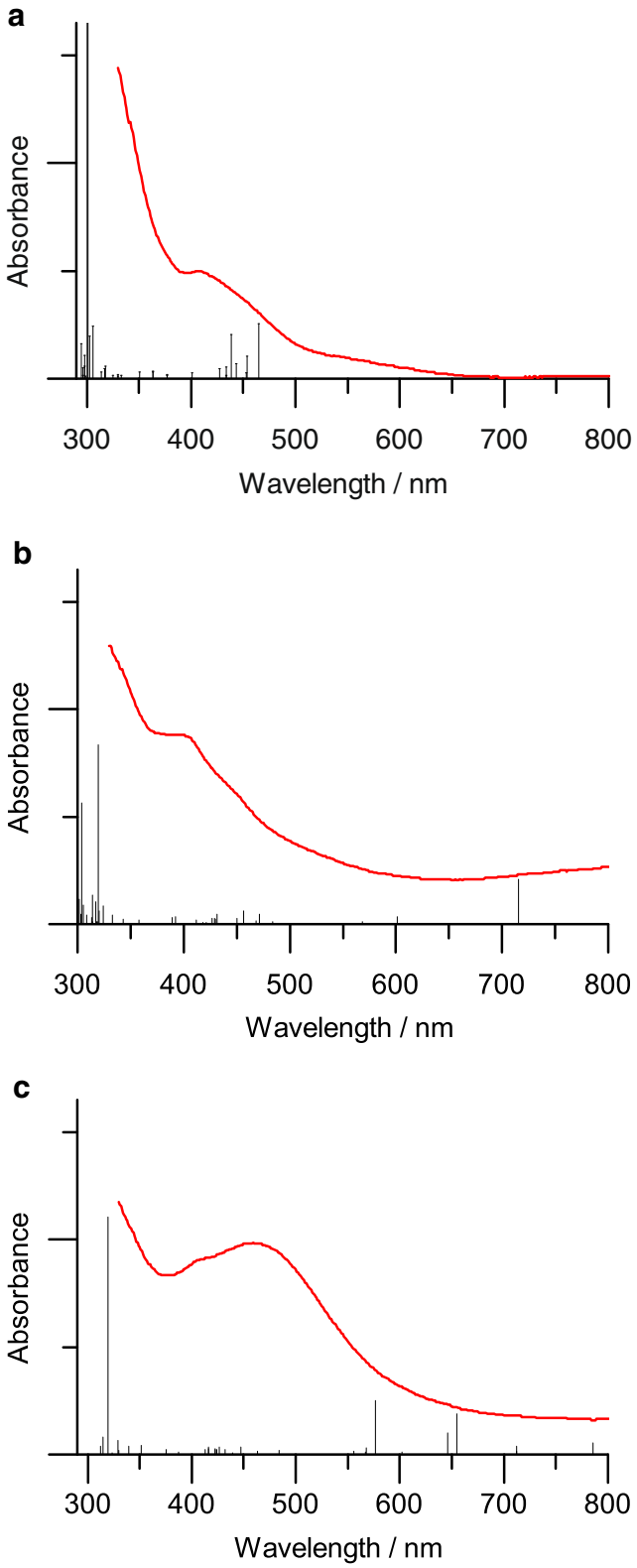

◀ **Fig. 4** Electronic spectra for $[Ni(SalEn)]_4^q$ (q=0 (**a**), 2+ (**b**), 4+ (**c**)) tetramers obtained from TD-DFT calculations. The curves are experimental spectra for poly[Ni(Salen)] film deposited on 2 cm^2 ITO glass. Spectra were recorded in situ at electrode potentials 0, 0.7, and 1.2 V (**a**, **b**, and **c**, respectively). The background electrolyte was 0.1 mol dm^{-3} N (Et) $_4BF_4$/CH_3CN. Polymer film was deposited by potentiostatic anodic oxidation at 1 V from the 1 mmol solution of monomer with background electrolyte. Surface coverage is 2.6×10^{-8} mol/cm^2

rings-rings and bridges-rings exchange. The intensive band observed at 576 nm for $[Ni(SalEn)]_4^{4+}$ also has a noticeable MLCT contribution, but is mostly associated with the charge transfer from the "inner" units of the tetramer to the "outer" ones. The high-energy bands for both oxidized forms of the tetramer are mostly LLCT with minor MLCT or LMCT contributions. The MLCT transitions found for $[Ni(SalEn)]_4^{2+}$ at 318 nm have very low intensity and are completely obscured by more intensive bands.

Thus, the TD-DFT calculations provide a reasonable description of the electronic spectrum of $[Ni(SalEn)]_4^0$. For $[Ni(SalEn)]_n^{2+}$ the DFT calculations reproduce adsorption in the near-IR range and the significant decrease of adsorption intensity around 300 nm. The important peculiarity of the spectrum for $[Ni(SalEn)]_4^{4+}$ is the complete absence of high-intensity transitions corresponding to the band observed in experimental spectra near 480 nm. As mentioned above, one can speculate that this band can only be observed in complexes with axial ligands, but an adequate computational proof of this hypothesis is not available yet.

The role of CH_3O groups in aromatic rings was studied for a series of dimeric complexes (Table 3). The spectra of reduced $[Ni(Schiff)]_2^0$ complexes are hardly affected by the presence of CH_3O groups, and show no perceptible solvatochromism. However, in the case of oxidized species, the substitution of 3-hydrogens in aromatic rings by CH_3O groups noticeably affects the position of near-infrared bands, showing a significant redshift for $[Ni(SalEn)]_2^{2+}$/$[Ni(CH_3OSalEn)]_2^{2+}$ and $[Ni(SaltmEn)]_2^{2+}$/$[Ni(CH_3OSaltmEn)]_2^{2+}$. The significant redshifting of the lowest-energy transitions can be explained by the fact that for $[Ni(CH_3OSchiff)]_2^{2+}$ complexes, the total charge on aromatic rings located between the metal centers is much higher (by ca. 0.3 e) than on the "outer" pair of aromatic rings. Therefore, the lowest-energy transition, which is interpreted as electron density transfer from the "outer" rings to the "inner" ones should proceed easier (i.e., with lower energy of transition) than for the corresponding $[Ni(CH_3OSchiff)]_2^{2+}$ complexes. The band near 600 nm is

Table 3 Wavelengths of absorption maxima (nm) in the electronic spectra of $[Ni(Schiff)]_2^{2+}$ and $[Ni(CH_3OSchiff)]_2^{2+}$ dimeric complexes obtained from DFT calculations

$[Ni(SalEn)]_2^{2+}$	325; 420; 595; 875; 1,595
$[Ni(SaltmEn)]_2^{2+}$	300; 425; 600; 865; 1,620
$[Ni(CH_3OSalEn)]_2^{2+}$	340; 440; 565; 995; 1,900
$[Ni(CH_3OSaltmEn)]_2^{2+}$	320; 410; 575; 850; 960; 1,700; 2,040

blueshifted by 20–30 nm upon addition of CH_3O-groups for oxidized dimeric complexes with both SalEn and SaltmEn.

Cyclic voltammetry and electrochemical quartz crystal microbalance

On cyclic voltammograms of unsubstituted poly[Ni(SalEn)] complex one can observe a pair of broad oxidation/reduction peaks (Fig. 5a).

Introduction of substituents into ligand structure of polymeric complexes leads to noticeable changes of voltammetric responses. Methyl substituents in imino bridges lead to a shoulder formation on both the anodic and cathodic branches of voltammograms (poly[Ni(SaltmEn)], Fig. 5b). Replacement of hydrogen by methoxy substituents in the aldehyde moiety leads to formation of additional peaks and shoulders, accompanied with shifts of polymer electroactivity regions in the cathodic direction (poly[Ni(CH_3OSalEn)], poly[Ni(CH_3OSaltmEn)], Fig. 5c, d). This is usually interpreted as a consequence of additional electrochemical processes, the nature of which is described in terms of structurally determined transport [10, 28] if a ligand-based electrochemical process is assumed, or in terms of combination of ligand- and metal-based oxidation processes [36, 37]. Voltamperometric measurements were performed at scan rates v from 5 to 200 mV/s. Dependencies of logarithm of peak current from the logarithm of the scan rate were studied for the pair of peaks at about 800 mV since other peaks are not well-pronounced for all scan rates. For the whole range of scan rates used these dependencies were linear, giving slopes of 0.8 for poly[Ni(SalEn)], 0.9 for poly[Ni(CH_3OSalEn)], 1.0 for poly[Ni(SaltmEn)], and 0.9 for poly[Ni(CH_3OSaltmEn)]. This means that peak currents I_p were almost proportional to the scan rate, corresponding to diffusionless behavior of the films. CV curves for different scan rates and the plots mentioned above can be found in Supplementary Information (Fig. S1 and S2).

The changes in geometry of the complexes predicted by DFT calculations may result in the shrinkage of the polymer film or, at least, in a change of the solvent flow during the first and second oxidation steps. To verify this assumption, electrochemical quartz crystal microbalance (EQCM) measurements were performed. The films were cycled at 25 mV/s in the potential range 0–1.2 V and massograms were recorded after stabilization of the CV curve, which is necessary due to

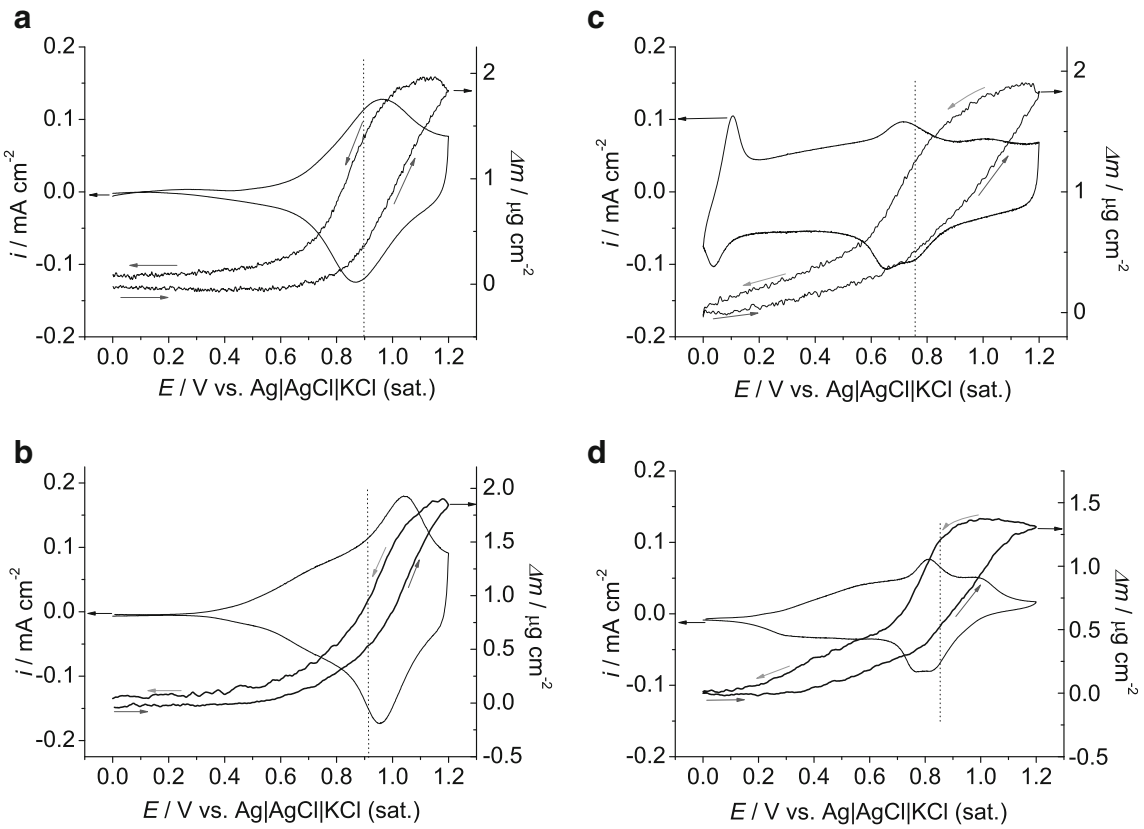

Fig. 5 Typical voltammograms of 1.37 cm^2 quartz crystal coated by electrodeposited polymeric complexes **a** poly[Ni(SalEn)], **b** poly[Ni(SaltmEn)], **c** poly[Ni(CH_3OSalEn)], **d** poly[Ni(CH_3OSaltmEn)] together with changes of polymer film mass. The background electrolyte was 0.1 mol dm^{-3} N (Et) $_4BF_4/CH_3CN$, scan rate is 0.025 V s^{-1}. Surface coverage is 3.8×10^{-8} mol/cm^2. *Dashed line* indicates the potential at which the mass of charge-compensated species is changing (see text for details), scan direction is indicated by *arrows*

the irreversible currents observed during the first cycles. Such currents are usually attributed to the polymer crosslinking. As demonstrated in Fig. 6, oxidation of the polymers is accompanied by an increase in their weight due to entry of charge-compensating ions and solvent molecules into the film, and the reduction is accompanied by withdrawal of the corresponding species from the film. Nevertheless, the molar weights of charge-transferring species depend on the polarization potential (as two linear regions can be found of Δm (q) curves, Fig. 6).

Doping level y of conducting polymers can be calculated from the ratio of polymerization charge q_{pol} and oxidation charge in monomer-free solution q_{redox} by the well-known formula $q_{pol}/q_{redox}=(2+y)/y$ [9]. It is worth noting that for all polymers in question the first linear region of Δm (q) curves suggests an oxidation charge of about 1 mC cm^{-2}, corresponding to the doping level in the range of 0.15–0.3. On the other hand, one can observe that polymers oxidized up to 1.2 V have quite different doping levels ranging from 0.4 to 0.9.

In Table 4, molar weights of charge-compensating species, calculated by standard procedure [38] from the slope of linear regions of mass Δm vs. charge q dependences are presented. For all polymers in question, two such linear regions are observed (Fig. 6). Under oxidation potentials below 0.8 V the injection of anionic species into the film is combined with the ejection of solvent particles from the film, as charge carriers molar masses are in all cases less than the mass of BF_4^- anion (81 g/mol). It corresponds to replacement of a solvent molecule by each charge-compensating anion, so we can assume that at this potential range film is quite dense and has not enough space to host BF_4^- anion with its solvate shell. If oxidation is continued to potentials up to 1.2 V, no solvent ejection is observed; the mass of charge-compensating species becomes higher than one of BF_4^- anion, so the flux of counterions can be accompanied by solvent injection. It is interesting that the mass of charge-compensating species is weakly dependent on the scan range (for details, see Table S1 and Fig. S3 in Supplementary Information), so we can conclude that the solvent uptake is not time-dependent, thus suggesting that the solvent transfer is not a straightforward result of a concentration gradient or physical opening/closing of the polymer. However, combined EQCM and probe-beam study

Table 4 Mass of charge-compensating species (g/mol) entering poly[Ni(Schiff)] films during their oxidation/reduction in different potential ranges. Masses are averaged over different scan rates (5–200 mV/s)

Polymer	Potential range	
	0–0.8 V	0.8–1.2 V
poly[Ni(CH_3OSaltmEn)]	54±6	166±26
poly[Ni(CH_3OSalEn)]	35±4	130±8
poly[Ni(SaltmEn)]	45±12	81±24
poly[Ni(SalEn)]	49±20	108±11

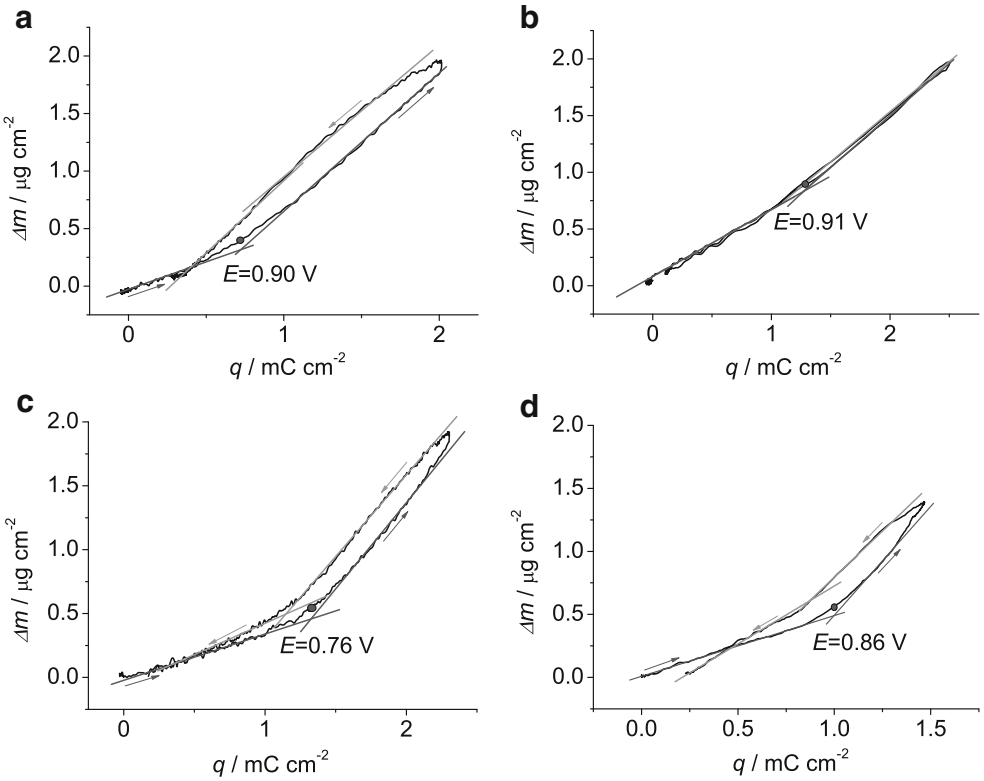

Fig. 6 Dependencies of polymer film mass (Δm) from the oxidation charge q, calculated from the data presented in Fig. 5: **a** poly[Ni(SalEn)], **b** poly[Ni(SaltmEn)], **c** poly[Ni(CH_3OSalEn)], **d** poly[Ni(CH_3OSaltmEn)]. The potential at which the mass of charge-compensated species is changing is shown on the graph; scan direction is indicated by *arrows*

of poly[Ni(SaltmEn)] films [11] and in situ ellipsometric study of [Pd(CH_3OSalEn)] films [13] performed by other groups have demonstrated similar features, including solvent injection and film expansion during the second oxidation step.

Limited information on the structural changes taking place in polymer films upon oxidation can be provided by DFT calculations, which predict noticeable changes in dihedral angles between monomer units in a chain upon oxidation (see "Geometry and electronic structure" section). This is likely to lead to better packing of polymer chains in the film and might eventually result in a more compact polymer structure. However, due to the limitations of the computational model, which does not explicitly take into account the counterions and solvent molecules, DFT results do not suggest a possible mechanism for the expansion of the film at higher oxidation potentials. Simulations of the polymer film behavior using a larger-scale model are clearly desirable to gain insight into the nature of structural transformations accompanying the oxidation process.

From voltammetric and EQCM measurements, it is clear that oxidation of the polymers in question proceeds by two steps. The charge, consumed during the first step, does not depend on ligand structure; during this step, solvent flow is opposite to counterion one. The second step is accompanied by solvent injection into the film; the charge consumed during this process depends on the ligand structure. To understand the nature of observed redox transformations, spectral methods will be used.

UV-visible spectroscopy

One of the most characteristic features of polymeric [Ni(Schiff)] complexes is their electrochromism, i.e., the ability to change their light absorbance in response to polarization. UV-visible spectroscopy of thin polymer films deposited on transparent electrodes is one of the most important characterization methods for electrochromic polymers. If electrochemical experiment is carried out in a photometric cell, in situ absorption spectra could be registered during potentiostatic polarization or cyclic voltammetry measurements, giving direct information about polymer structure at any oxidation state, provided that such states have absorption bands in visible, UV, or near-infrared ranges.

Characteristic spectra of poly[Ni(SalEn)] films, measured at potentiostatic polarization from 0 V to 1.2 V, are presented on Fig. 7. A reduced form of the polymer (*Red*) has a characteristic absorption band at 406 nm and a strong band in UV range, which cannot be resolved due to the limitations of the experimental setup (namely, high ITO glass absorption in UV range). During the oxidation of the polymer, new absorption bands appear. At potentials less than 0.9 V, a wide near-infrared band is observed. Simultaneous growth of the 406 nm band is observed during this oxidation stage.

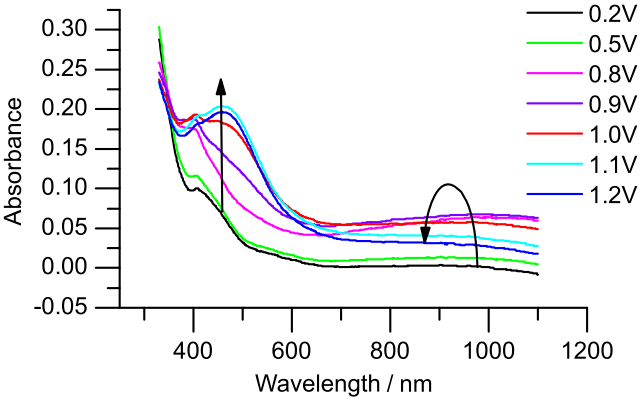

Fig. 7 Characteristic spectra of poly[Ni(SalEn)] films deposited on 2 cm^2 ITO glass, measured at potentiostatic polarization from 0 V to 1.2 V (vs. Ag/AgCl). Direction of absorption maxima evolution with increase of the electrode potential is indicated by *arrows*. Spectra were recorded in situ, the background electrolyte is 0.1 mol dm^{-3} N (Et) $_4BF_4$/CH_3CN, surface coverage is 2.6×10^{-8} mol/cm^2

Intensities of these bands increase, and the wavelength of near-infrared band maximum shifts from 900 to 1,000 nm with increase of film potential up to 0.96 V. On the basis of earlier studies of monomeric complexes [18, 20–22] and our DFT calculations, this band can be interpreted as a low-energy LLCT transition. Similar bands were observed for conjugated polymers, such as polythiophenes [39]. So, the growth of this absorption band may be attributed to formation of the first oxidized form of the polymer, *Ox1*, for which the electron density is highly delocalized on the phenyl moieties of the ligand. In terms of conducting polymers model, this kind of electronic structure can be described as a polaron. Such spectra of delocalized structure are in reasonable agreement with our DFT calculations (see "Electronic spectra" section).

At potentials higher than 0.9 V, some decrease of absorption bands at 406 nm and in near-infrared range is observed, together with an increase of absorbance at 460 nm, at polarizations higher than 1 V leading to the formation of a well-defined band. The interpretation of this band in SalEn-type polymeric complexes is questionable: in the literature, it has been assigned either to MLCT [10, 28] or to the transition valence band→antibonding bipolaron level *y* [9]. In both cases, the charge was assumed to be delocalized over the phenyl rings. However, our DFT calculations ("Electronic spectra" section), describing polymers with delocalized charge, do not predict any intense band in this region, so we refer to the data obtained for monomeric complexes [18, 20–22], where the authors proved that the appearance of such MLCT band corresponds to localization of charge density on Ni atom in the presence of axial ligands. It means that at high potentials the formation of the second, metal-based oxidized form of polymer (*Ox2*) is plausible. In this case, we should assume that the existence of such form is possible if the axial positions at the Ni atom are occupied by some ligands, as it was observed for monomeric SalEn-type

complexes [18, 20–22]. A decrease of the first oxidized form bands responds to the transformation of the first oxidized form (*Ox1*) to *Ox2*. In the spectra of substituted polymers, one can observe the same kinds of absorption bands having the same behavior with increasing film potentials (Fig. 8).

It may be noted that introduction of methoxy substituents into the aldehyde moiety leads to the redshift of the middle-range band from 460 to 580 nm. At the same time, no shift of the band at 406 nm is observed. Near-infrared band has a blueshift, which is not well-pronounced due to the extremely large width of this band (see Fig. 8).

To explain the formation of intense bands in the region 460–600 nm in terms of localization of charge on the metal center we have assumed that moderately coordinating solvents such as acetonitrile may act as axial ligands in case of studied polymer films. To check this assumption, we have recorded ex situ spectra of reduced and oxidized form of poly[Ni(CH_3OSalEn)], which has the most distinct near-infrared and visible bands. Films were tested in solutions of Et_4NBF_4 in acetonitrile and dichloromethane, the latter not being a coordinating solvent. To exclude the influence of traces of water, which may also act as axial ligand, films were electrochemically oxidized in nitrogen (99.9999 %)-filled glovebox, sealed in the photometric cell and immediately transferred into the spectrophotometer (Fig. 9, curve 1). One can note that only the low-energy LLCT band is formed after oxidation of polymer in dichloromethane and no band in the vicinity of 500 nm is observed even at high oxidation potential. Ex situ spectrum in acetonitrile solution (Fig. 9, curve 2) demonstrates strong band at 580 nm and correlates with the in situ one (Fig. 8c), justifying our technique.

On the other hand, if the film, oxidized in acetonitrile, is removed from the cell and dried under vacuum without exposure to the air, rapid decrease of a band at 580 nm is observed together with growth of near-infrared band (Fig. 9, curve 3). Obtained spectra of dry films demonstrate absorption bands at 310, 400, 565 (shoulder), and 850 nm, coinciding with calculated ones (see Table 3), similar bands are observed if polymers are oxidized in dichloromethane. It means that charge in dry oxidized polymers, as well as in ones treated in dichloromethane, is delocalized over the phenyl rings, as it was predicted by DFT calculations. Using of supporting electrolyte based on coordinating solvent such as acetonitrile leads to different absorption spectra of oxidized polymers, corresponding to the shift of oxidation locus to the Ni center.

These observations demonstrate the crucial role of a coordinating solvent in the stabilization of the second oxidized

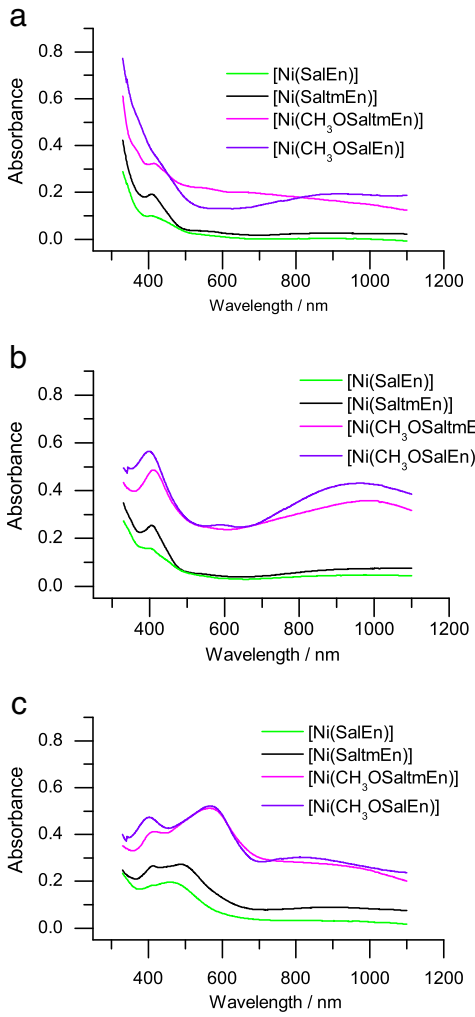

Fig. 8 UV-visible adsorption spectra of poly[Ni(Schiff)] complexes, recorded at polarization of polymer film at potentials **a** 0.2 V, **b** 0.7 V, **c** 1.2 V (vs. Ag/AgCl). Experimental conditions were the same as for Fig. 7, polymer abbreviations are presented on the plot

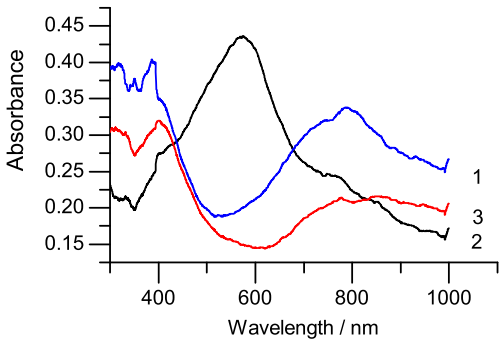

Fig. 9 Characteristic spectra of 2 cm^2 ITO glass modified by the oxidized form of poly[Ni(CH_3OSalEn)], measured ex situ after potentiostatic polarization at given potential value. In each case, oxidation was performed inside the photometric cell, placed in the dry nitrogen-filled glovebox. The cells were sealed inside the glovebox together with working solution (*curves 1–2*) and than moved into spectrophotometer. Oxidation was performed in: 0.1 mol dm^{-3} N (Et) $_4BF_4$/dichloromethane solution, oxidation potential 1.4 V (*curve 1*); 0.1 mol dm^{-3} N (Et) $_4BF_4$/acetonitrile solution, oxidation potential 1.3 V (*curve 2*). *Curve 3* represents the spectrum of the same film obtained after removing it from the solution and drying under vacuum inside the glovebox. Electrode with the film was sealed in the dry photometric cell inside the glovebox before measurement. Polymerization conditions are the same as in Fig. 7

form of polymer. Due to this reason, the oxidation state of nickel in the films, treated in solutions, cannot be directly correlated with one detected in dry films by any ex situ methods that can discriminate between Ni(II) radicals and Ni(III) species, such as EPR, X-ray absorption, or X-ray photoelectron spectroscopy. Identification of metal electronic structure in the second oxidation form must be based only on in situ methods and DFT calculations with a solvent coordinated to the axial position of metal atom, which, together with a detailed study of solvent effects, will be published separately.

Here, we want to conclude that oxidation of SalEn-type polymeric nickel complexes proceeds in two steps. The reduced form of the polymer is first oxidized to the *Ox1* form, which is characterized by charge delocalization over the conjugated bonds system of the polymer. Subsequent oxidation in acetonitrile solutions leads to formation of the second oxidized form, *Ox2*, for which the spectra cannot be described in terms of delocalized charge, but correlate with charge localization on metal atom, stabilized by axial coordination of a solvent.

Voltabsorptometry

Simultaneous registration of cyclic voltammograms and light absorption on selected wavelengths can be used to characterize the trends of discussed transformations between one reduced and two oxidized forms of polymers. Detailed dependences of absorption on selected wavelengths vs. electrode potential are presented in Supplementary Information (Fig. S4).

At the potential scan in positive direction, initially the *Ox1* form is produced. Increase in potential leads to formation of the *Ox2* form, followed by decrease in absorption bands of the first oxidized form of the polymer. One can notice a similar behavior of absorption bands in near-infrared range and ones at approximately 400 nm, which confirms their assignment to the same form of the polymer. At high potentials, absorption of the *Ox1* and *Ox2* forms tends to constant non-zero values, so one may assume that if polymers in question are completely oxidized, they contain both oxidized forms and some charge delocalization in phenyl moieties exists.

To prove that electrochemical response of the polymeric film is determined by transition of the *Red* form into the *Ox1* and *Ox2* ones together with conversion of oxidized forms one into another, we have used a combination of the Beer–Lambert and Faraday laws. According to the Beer–Lambert law, absorbance of a substance is proportional to concentration and the distance the light travels through the material (which is a polymer film thickness in our case):

$$A_i = C_i l \varepsilon_i, = n_i \varepsilon_i / s, \tag{1}$$

where s is the light beam cross section area, C_i is the concentration of optically active sites on the electrodes (i.e., optically active polymer fragments in the film), $n_i = slC_i$ is the quantity of ith species in the part of the film with thickness l and surface area s; A_i, ε_i—absorbance and extinction coefficient of ith species at selected wavelength, respectively, i=*Ox1*, *Ox2*; l, path length of light, which is equal to polymer film thickness. In the calculations, the extinction coefficients are assumed to be independent of the charge state of the film.

If we assume that the number of electroactive species and extinction coefficients ε_i are constant, absorbance time derivative, dA/dt, can be used to obtain partial currents resulting from electrochemical transformations of each polymer form: Eq. (1) derives to

$$\frac{dA_i}{dt} = \frac{dn_i \varepsilon_i}{dt\ s}. \tag{2}$$

Partial current caused by electrochemical formation of $n_i = slC_i$ moles of species i is equal to

$$I_i = \frac{dQ_i}{dt} = nF\frac{dn_i}{dt}, \tag{3}$$

where n is the number of electrons transferred in the reaction, F is the Faraday constant, Q_i is the charge consumed for redox switching. Thus, taking into account Eq. (2), we can correlate the partial current and absorbance time derivative

$$I_i = \frac{snF}{\varepsilon_i}\frac{dA_i}{dt}, \tag{4}$$

so the overall current in the model of formation of two oxidized species *Ox1* and *Ox2* should be equal to

$$I = snF\left(\frac{dA_{\mathrm{Ox1}}}{dt}\frac{1}{\varepsilon_{\mathrm{Ox1}}} + \frac{dA_{\mathrm{Ox2}}}{dt}\frac{1}{\varepsilon_{\mathrm{Ox2}}}\right). \tag{5}$$

As the bands of two oxidized forms are well-defined, assuming overlapping effects to be negligible, one can use absorbances at the peak of characteristic bands (900–1,000 nm for the *Ox1* form and 450–550 nm for the *Ox2* form), corrected on the spectra of the reduced form as a baseline, to calculate partial currents according to Eqs. (4–5). In general case, voltammetric curve may be just fitted according to Eq. (5), but at least one of the extinction coefficients can be easily determined from dependencies of absorbance responses and charges

(integrated currents) q, consumed for redox switching according to the relation

$$Q_i = \frac{snF}{\varepsilon_i} A_i \tag{6}$$

In the simplest case of two ideal interconverting species a plot of A_i vs Q_i should be linear with the slope of $\frac{\varepsilon_i}{snF}$. Formation of additional species may lead to curvature of the plot or to a linear dependence with a different slope. In such case it is justified to use Eq. (6) for the systems in question only in the range of formation of the form *Ox1* and only until it starts to convert to form *Ox2*. To obtain extinction coefficient of *Ox2* form (or, in general case, all other forms), it is possible to use iteration method. Using the $\frac{\varepsilon_{Ox1}}{snF}$ values obtained, one can calculate partial current of formation or transformation of *Ox1* for the whole potential range by means of Eq. (4). Such partial currents can be subtracted from voltammetric curve. As a result, partial voltammogram of formation or transformation of *Ox2* will be obtained (see Eq. (5)). It can be treated according to Eq. (6) in order to obtain the extinction coefficient of the *Ox2* form. Full derivative voltabsorptograms calculated by Eq. (5) will contain all partial currents of formation and conversion of two oxidized forms, detected by UV-visible spectroscopy. Such curves for all polymers in question are presented in Fig. 10 and the extinction coefficients are listed in Table 5. The procedures for determining the extinction coefficients and constructing the partial voltammograms are described in more detail in Supplementary Information.

Table 5 Extinction coefficients for poly[Ni(SalEn)] species. Wavelengths are given in parenthesis

Polymer complex	Extinction coefficient, mol^{-1} m^2
poly[Ni(SalEn)]	900 (460 nm), 600 (990 nm)
poly[Ni(SaltmEn)]	1600 (490 nm), 1200 (990 nm)
poly[Ni(CH_3OSalEn)]	1700 (580 nm), 2000 (970 nm)
poly[Ni(CH_3OSaltmEn)]	1300 (540 nm), 1500 (1,016 nm)

One can note good correlation between voltabsorptograms and voltammograms. Both types of curves contain the same number of peaks with the same peak potentials characteristic for each polymer in question. Currents, predicted from spectral data, are close to the measured electric currents. In this case, we may assume that the model of formation of two interconverting optically active oxidized forms is sufficient to describe complicated voltamperic response of studied complexes, regardless of substituent origin.

Figure 11 demonstrates the influence of ligand substituents on the formation of each oxidized form. Partial voltammograms of the *Ox1* form are complicated by its conversion to the *Ox2* form, which results in negative currents at positive potential scans and vice versa. Such features prevent formation of clear voltammetric peaks on the *Ox1* partial voltammograms. For all studied complexes, formation of the first oxidized form is shifted for about 200 mV to the cathodic region by introduction of methoxy substituents in the aldehyde moiety (Fig. 11a, b). Peak currents of *Red* ↔ *Ox1* transitions (points 1, 1′ on the figure) are influenced neither

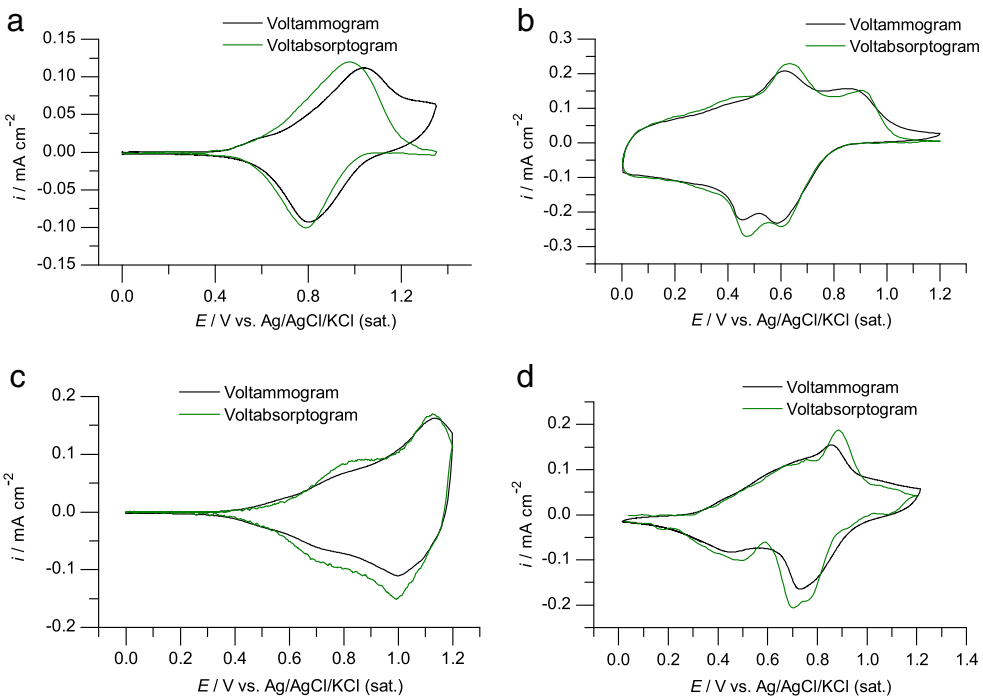

Fig. 10 Comparison of voltammograms and voltabsorptograms for polymeric complexes: **a** poly[Ni(SalEn)], **b** poly[Ni(CH_3OSalEn)], **c** poly[Ni(SaltmEn)], **d** poly[Ni(CH_3OSaltmEn)]. Potential scan rate is 20 mV/s. Experimental conditions were the same as indicated in Fig. 7

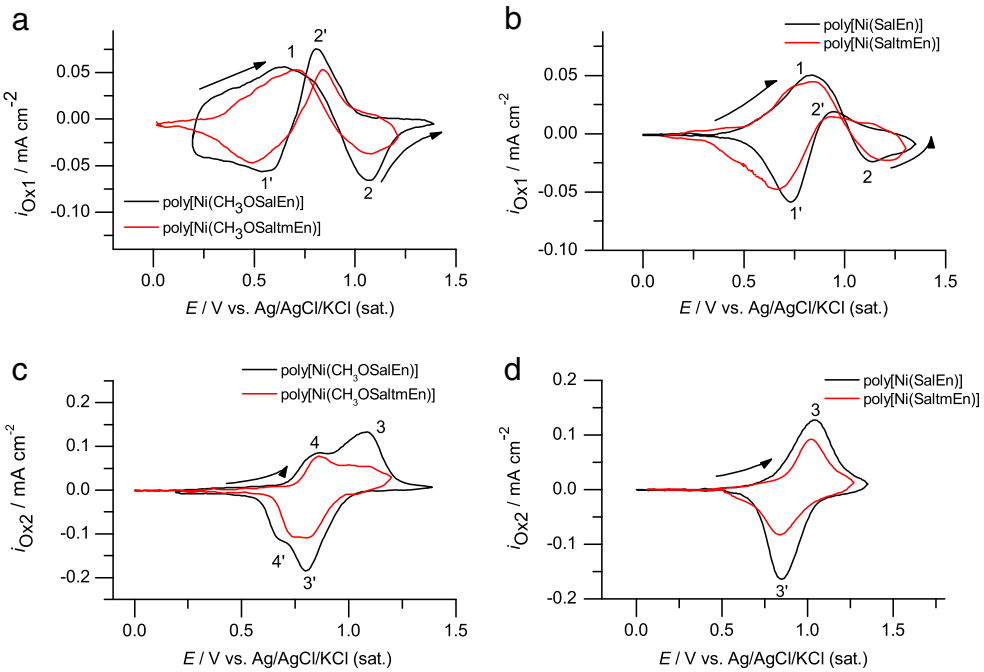

Fig. 11 Partial voltammograms, calculated from light absorption at 970 nm (**a**, **b**) and 580 nm (**c**, **d**) for polymer films of [Ni(Schiff)] complexes. Film compositions are presented on the graphs, numbers indicate peaks discussed in the text. Direction of the potential scan is indicated by *arrows*. Experimental conditions were the same as indicated in Fig. 7

by methoxy substituents in the aldehyde moiety, nor by methyl substituents in the imino bridges. Anodic limit of the *Ox1* stability, according to the presented data, is about 0.8–0.9 V. Comparing the above observations with EQCM and coulometric data ("Cyclic voltammetry and electrochemical quartz crystal microbalance" section) one can find coincidence between the first process, observed on EQCM, and formation of the *Ox1* form of polymer, described by spectral data.

At the same time, currents resulting from the *Ox1* to *Ox2* transformation (points 2, 2′) are increased with the introduction of methoxy substituents. It corresponds to a higher degree of conversion between oxidized forms of methoxy substituted polymers. Partial voltammograms of the *Ox2* form (Fig. 11c, d) contain one pair of wide peaks (points 3, 3′) at 940 mV if the monomer unit does not contain methoxy substituents. If such substituents are introduced into the aldehyde moiety, the second pair of peaks appears at 770 mV (points 4, 4′). Such peak splitting may be attributed to the two different ways of the *Ox2* formation. Peaks 3, 3′ have the same potentials as the peaks of the *Ox1* to *Ox2* transformation on the *Ox1* partial voltammogram (points 2, 2′ in Fig. 11a, b), so they correspond to formation of the *Ox2* form from the *Ox1* form. Peaks 4,4′ do not correlate with any peaks of *Ox1* partial voltammograms, so they may be assigned to formation of *Ox2* form directly from *Red* form. Introduction of methyl substitutes in the imino bridges does not affect the position of any peaks, but decreases intensity of the peaks at 940 mV. Features of the *Ox2* formation process, revealed by spectral data, allow one to correlate it with the second oxidation step, described by EQCM technique. Solvent injection, observed in the course of this process justifies our assumption about solvent role in stabilization of the *Ox2* form. If we assume that axial coordination of solvent molecules or phenyl rings of neighboring polymer layers on metal center is important for formation of Ni(III) species, then current decrease with introducing substituents into imino bridge may be explained by steric obstacles, produced by methyl groups.

Conclusions

Redox transformation of various polymeric [Ni(SalEn)] type complexes were studied by cyclic voltammetry, UV-visible spectroscopy, in situ derivative voltabsorptometry, and electrochemical quartz crystal microbalance, and compared with DFT calculation predictions. It was demonstrated that in acetonitrile-based supporting electrolyte solutions oxidation of such complexes, regardless of ligand substituents, proceeds by two routes, leading to formation of the two oxidized forms *Ox1* and *Ox2*. Complicated electrochemical response of studied substituted polymers can be explained in scope of this model without any additional assumptions, taking into account interconversion of the forms *Ox1* and *Ox2*. Formation of the first form and its characteristics are in good correlation with DFT calculations, performed for a chain model of polymer. According to calculation results, the charge in this case is delocalized on the ligand and thus the *Ox1* form can be easily assigned to polaron in terms of conducting polymers charge transfer model. Such delocalization is observed in dry polymers, or in polymers, treated in non-coordinating solvent, even at high oxidation potentials. On the other hand, in

coordinating solvent the second oxidized form of polymers can be observed. This form is not predicted by calculations using the simple chain model of polymer, and the role of the solvent in its formation has not been described before for polymeric complexes of this type. However, the spectral properties of the oxidized polymers in acetonitrile solutions correlate with observations of Ni(III) species made on monomeric complexes with axial ligands [18, 20–22]. Acetonitrile and phenyl moieties of neighboring polymer layers may act as such ligands. The in-depth understanding of the demonstrated effects of axial ligands and solvent on the oxidation route of the complexes studied may provide an efficient way of controlling the catalytic properties and stability of the complexes.

Acknowledgments This research was supported by the Russian Foundation for Basic Research (grant # 13-03-00843-a). V.V.M. would like to acknowledge the funding from the Russian Foundation for Basic Research (grant # 12-03-00560-a) and St. Petersburg State University (grant # 12.38.77.2012). DFT calculations were performed using the facilities provided by the Computational Resource Center of St. Petersburg State University. The authors wish to thank Prof. Larry Daniels (Wake Forest University, USA) for very constructive comments.

References

1. Popeko IE, Vasilev VV, Timonov AM, Shagisultanova GA (1990) Electrochemical-behavior of palladium (II) complexes with schiff-bases and synthesis of Pd (II)-Pd (IV) mixed-ligand complex. Zh Neorg Khim 35:933–937
2. Dahm CE, Peters DG (1996) Catalytic reduction of α, ω-dihaloalkanes with nickel (I) salen as a homogeneous-phase and polymer-bound mediator. J Electroanal Chem 406:119–129
3. Dahm CE, Peters DG, Simonet J (1996) Electrochemical and spectroscopic characterization of anodically formed nickel salen polymer films on glassy carbon, platinum, and optically transparent tin oxide electrodes in acetonitrile containing tetramethylammonium tetrafluoroborate. J Electroanal Chem 410:163–171
4. Leung ACW, Maclachlan MJ (2007) Schiff base complexes in macromolecules. J Inorg Organomet Polymers Mater 17:57–89
5. Gao F, Li JL, Kang FY, Zhang YK, Wang XD, Ye F, Yang J (2011) Preparation and characterization of a poly[Ni(salen)]/multiwalled carbon nanotube composite by in situ electropolymerization as a capacitive material. J Phys Chem C 115:11822–11829
6. Popeko IE, Timonov AM, Shagisultanova GA (1990) Electrocatalytic properties of a chemically modified electrode based on the Pd (IV)-Pd (II) complex with Bis (Salicylidene)-ethylenediamine. J Appl Chem USSR 63:2033–2036
7. Chepurnaya IA, Logvinov SA, Karushev MP, Timonov AM, Malev VV (2012) Modification of supercapacitor electrodes with polymer metallocomplexes: methods and results. Russ J Electrochem 48:538–544
8. Zhang YK, Li JL, Gao F, Kang FY, Wang XD, Ye F, Yang J (2012) Electropolymerization and electrochemical performance of salen-type redox polymer on different carbon supports for supercapacitors. Electrochim Acta 76:1–7
9. Vilas-Boas M, Freire C, De Castro B, Christensen PA, Hillman AR (1997) New insights into the structure and properties of electroactive polymer films derived from [Ni(salen)]. Inorg Chem 36:4919–4929
10. Vilas-Boas M, Santos IC, Henderson MJ, Freire C, Hillman AR, Vieil E (2003) Electrochemical behavior of a new precursor for the design of poly[Ni(salen)]-based modified electrodes. Langmuir 19:7460–7468
11. Vilas-Boas M, Henderson MJ, Freire C, Hillman AR, Vieil E (2000) A combined electrochemical quartz-crystal microbalance probe beam deflection (EQCM-PBD) study of solvent and ion transfers at a poly[Ni(saltMe)]-modified electrode during redox switching. Chem Eur J 6:1160–1167
12. Vilas-Boas M, Freire C, De Castro B, Christensen PA, Hillman AR (2001) Spectroelectrochemical characterisation of poly[Ni(saltMe)]-modified electrodes. Chem Eur J 7:139–150
13. Hamnett A, Abel J, Eameaim J, Christensen P, Timonov A, Vasilyeva S (1999) A study of the polymerisation and electrochemical cycling of Pd methoxy-Salen derivatives using fast ellipsometry and FT-infrared spectroscopy. Phys Chem Chem Phys 1:5147–5156
14. Shimazaki Y, Yajima T, Tani F, Karasawa S, Fukui K, Naruta Y, Yamauchi O (2007) Syntheses and electronic structures of one-electron-oxidized group 10 metal (II)-(disalicylidene) diamine complexes (metal = Ni, Pd, Pt). J Am Chem Soc 129:2559–2568
15. Shimazaki Y, Stack TDP, Storr T (2009) Detailed evaluation of the geometric and electronic structures of one-electron oxidized group 10 (Ni, Pd, and Pt) metal (II)-(disalicylidene) diamine complexes. Inorg Chem 48:8383–8392
16. Orio M, Jarjayes O, Kanso H, Philouze C, Neese F, Thomas F (2010) X-ray structures of copper (II) and nickel (II) radical salen complexes: the preference of galactose oxidase for copper (II). Angew Chem Int Ed 49:4989–4992
17. Storr T, Wasinger EC, Pratt RC, Stack TDP (2007) The geometric and electronic structure of a one-electron-oxidized nickel (II) bis (salicylidene) diamine complex. Angew Chem Int Ed 46:5198–5201
18. Shimazaki Y, Tani F, Fukui K, Naruta Y, Yamauchi O (2003) One-electron oxidized nickel (II)-(disalicylidene) diamine complex: temperature-dependent tautomerism between Ni(III)-phenolate and Ni(II)-phenoxyl radical states. J Am Chem Soc 125:10512–10513
19. Rotthaus O, Jarjayes O, Perez Del Valle C, Philouze C, Thomas F (2007) A versatile electronic hole in one-electron oxidized Ni^{II}bis-salicylidene phenylenediamine complexes. Chem Commun 43:4462–4464
20. Bag B, Mondal N, Rosair G, Mitra S (2000) The first thermally-stable singly oxo-bridged dinuclear Ni(III) complex. Chem Commun: 1729–1730
21. Rotthaus O, Jarjayes O, Thomas F, Philouze C, Valle CPD, Saint-Aman E, Pierre JL (2006) Fine tuning of the oxidation locus, and electron transfer, in nickel complexes of pro-radical ligands. Chem Eur J 12:2293–2302
22. Rotthaus O, Thomas F, Jarjayes O, Philouze C, Saint-Aman E, Pierre JL (2006) Valence tautomerism in octahedral and square-planar phenoxyl-nickel (II) complexes: are imino nitrogen atoms good friends? Chem Eur J 12:6953–6962
23. Goldsby KA, Blaho JK, Hoferkamp LA (1989) Oxidation of nickel (II) bis (salicylaldimine) complexes: solvent control of the ultimate redox site. Polyhedron 8:113–115
24. Dolphin D, Niem T, Felton RH, Fujita I (1975) Reversible intramolecular electron transfer in an oxidized nickel porphyrin. J Am Chem Soc 97:5288–5290
25. Seth J, Palaniappan V, Bocian DF (1995) Oxidation of nickel (II) tetraphenylporphyrin revisited. Characterization of stable nickel (III) complexes at room temperature. Inorg Chem 34:2201–2206
26. Rodyagina TY, Gaman'kov PV, Dmitrieva EA, Chepurnaya IA, Vasil'eva SV, Timonov AM (2005) Structuring redox polymers poly[M (schiff)] (M = Ni, Pd; Schiff = schiff bases) on a molecular level: methods and results of an investigation. Russ J Electrochem 41:1101–1110
27. Robin MB, Day P (1968) Mixed-valence chemistry: a survey and classification. Adv Inorg Chem Radiochem 10:247–422
28. Tedim J, Patricio S, Fonseca J, Magalhaes AL, Moura C, Hillman AR, Freire C (2011) Modulating spectroelectrochemical properties of

[Ni(salen)] polymeric films at molecular level. Synth Met 161: 680–691
29. Pfeiffer P, Breith E, Lübbe E, Tsumaki T (1933) Tricyclische orthokondensierte Nebenvalenzringe. Just Liebigs Ann der Chemie 503:84–130
30. Becke AD (1993) Density-functional thermochemistry. 3. The role of exact exchange. J Chem Phys 98:5648–5652
31. Lee CT, Yang WT, Parr RG (1988) Development of the Colle-Salvetti correlation-energy formula into a functional of the electron-density. Phys Rev B 37:785–789
32. Stephens PJ, Devlin FJ, Chabalowski CF, Frisch MJ (1994) Ab-initio calculation of vibrational absorption and circular-dichroism spectra using density-functional force-fields. J Phys Chem 98:11623–11627
33. Dunning TH Jr, Hay PJ (1977) Gaussian basis sets for molecular calculations. In: Schaefer H III (ed) Methods of electronic structure theory. Springer, New York, pp 1–27
34. Hay PJ, Wadt WR (1985) Ab initio effective core potentials for molecular calculations—potentials for K to Au including the outer-most core orbitals. J Chem Phys 82:299–310
35. Frisch MJ, Trucks GW, Schlegel HB, Scuseria GE, Robb MA, Cheeseman JR, Scalmani G, Barone V, Mennucci B, Petersson GA, Nakatsuji H, Caricato M, Li X, Hratchian HP, Izmaylov AF, Bloino J, Zheng G, Sonnenberg JL, Hada M, Ehara M, Toyota K, Fukuda R, Hasegawa J, Ishida M, Nakajima T, Honda Y, Kitao O, Nakai H, Vreven T, Montgomery JA, Peralta JE, Ogliaro F, Bearpark M, Heyd JJ, Brothers E, Kudin KN, Staroverov VN, Kobayashi R, Normand J, Raghavachari K, Rendell A, Burant JC, Iyengar SS, Tomasi J, Cossi M, Rega N, Millam JM, Klene M, Knox JE, Cross JB, Bakken V, Adamo C, Jaramillo J, Gomperts R, Stratmann RE, Yazyev O, Austin AJ, Cammi R, Pomelli C, Ochterski JW, Martin RL, Morokuma K, Zakrzewski VG, Voth GA, Salvador P, Dannenberg JJ, Dapprich S, Daniels AD, Farkas, Foresman JB, Ortiz JV, Cioslowski J, Fox DJ (2009) Gaussian 09, Revision C.01
36. Levin OV, Karushev MP, Timonov AM, Alekseeva EV, Zhang SH, Malev VV (2013) Charge transfer processes on electrodes modified by polymer films of metal complexes with Schiff bases. Electrochim Acta 109:153–161
37. Malev VV, Levin OV, Timonov AM (2013) Quasi-equilibrium voltammetric curves resulting from the existence of two immobile charge carriers within electroactive polymer films. Electrochim Acta 108:313–320
38. Krasikova SA, Besedina MA, Karushev MP, Dmitrieva EA, Timonov AM (2010) In situ electrochemical microbalance studies of polymerization and redox processes in polymeric complexes of transition metals with Schiff bases. Russ J Electrochem 46:218–226
39. Tolstopyatova EG, Pogulaichenko NA, Eliseeva SN, Kondratiev VV (2009) Spectroelectrochemical study of poly-3,4-ethylenedioxythiophene films in the presence of different supporting electrolytes. Russ J Electrochem 45:252–262